Revised Manuscript (Unmarked)

Controllable Ligand Spacing Stimulates Cellular Mechanotransduction and Promotes Stem Cell Osteogenic Differentiation on Soft Hydrogels

Man Zhang,[abc] Qian Sun,[a] Yiling Liu,[a] Zhiqin Chu,[d] Leixiao Yu,[e] Yong Hou,[e] Heemin Kang,[f] Qiang Wei,*[ag] Weifeng Zhao,*[a] Joachim P. Spatz,[bc] Changsheng Zhao [ag] and Elisabetta A. Cavalcanti-Adam[bc]

[a.] *College of Polymer Science and Engineering, State Key Laboratory of Polymer Materials and Engineering, Sichuan University, 610065 Chengdu, China*

[b.] *Department of Cellular Biophysics, Max Planck Institute for Medical Research, Jahnstraße 29, 69120, Heidelberg, Germany*

[c.] *Department of Biophysical Chemistry, Heidelberg University, INF 253, 69120, Heidelberg, Germany*

[d.] *Department of Electrical and Electronic Engineering, Joint Appointment with School of Biomedical Sciences, The University of Hong Kong, Pokfulam Road, Hong Kong, China*

[e.] *Institute of Chemistry and Biochemistry, Freie Universität Berlin, Takustr. 3, 14195 Berlin, Germany*

[f.] *Department of Biomicrosystem Technology, Korea University, Seoul, 02841 Republic of Korea*

[g.] *College of Biomedical Engineering, Sichuan University, 610064 Chengdu, China*

**Corresponding author. Sichuan University, College of Polymer Science and Engineering, State Key Laboratory of Polymer Materials and Engineering, 610065, Chengdu, China. E-mail address: wei@scu.edu.cn.*

***Corresponding author. Sichuan University, College of Polymer Science and Engineering, State Key Laboratory of Polymer Materials and Engineering, 610065, Chengdu, China. E-mail address: zhaoscukth@163.com.*

Abstrate

Hydrogels with tunable mechanical properties have provided a tremendous opportunity to regulate stem cell differentiation. Hydrogels with osteoid (about 30-40 kPa) or higher stiffness are usually required to induce the osteogenic differentiation of mesenchymal stem cells (MSCs). It is yet difficult to achieve the same differentiation on very soft hydrogels, because of low environmental mechanical stimuli and restricted cellular mechanotransduction. Here, we modulate cellular spatial sensing of integrin-adhesive ligands via quasi-hexagonally arranged nanopatterns to promote cell mechanosensing on hydrogels having low stiffness (about 3 kPa). The increased interligand spacing has been shown to regulate actomyosin force loading to recruit extra integrins on soft hydrogels. It

therefore activates mechanotransduction and promotes the osteogenic differentiation of MSCs on soft hydrogels to the level comparable with the one observed on osteoid stiffness. Our work opens up new possibilities for the design of biomaterials and tissue scaffolds for regenerative therapeutics.

Keywords: Ligand spacing; Mechanotransduction; Mesenchymal stem cell; Differentiation; Hydrogel

1. Introduction

Bone tissue transplantation presents many problems due to the source limitation and the risk of infection and immunogenicity [1]. Biomaterials used as artificial extracellular matrix (ECM) play an important role to regulate stem cell differentiation, providing tremendous promise for regenerative therapies [2].

Stem cells are surrounded by ECM *in vivo*, which provides both biochemical factors (chemical composition, molecular chirality, growth factors, etc.) [3] and physical cues (matrix elasticity, surface topography, ligand dynamics, and etc.) [4, 5], i.e. microniche, to mediate biological processes [6], Besides biochemical factors, physical cues regulate cell behaviors and fate determination alone or synergistically [7-10]. Substrate stiffness is one of the major factors, which can be easily controlled and has been widely considered to regulate stem cell differentiation.[11, 12] It has been shown that stem cells cultured on hydrogels with stiffness above 30 kPa undergo osteogenic differentiation, while adipogenic differentiation is favored on the soft hydrogels with stiffness lower than 10 kPa [13-17].

Cells sense and respond to microniche mechanics via mechanotransduction, which converts mechanical cues into biochemical signals [18]. Normally, only the substrates matching the stiffness of osteoid tissue (about 30 kPa) or higher stiffness stimulate the generation of intracellular force based on the formation of actomyosin cytoskeleton. The force-induced signaling cascades are further initiated to regulate transcription factors and activate the expression of osteogenic genes. However, the high stiffness of hydrogels is achieved by either high concentration of backbone polymers or high degree of crosslinking. The degradation of such stiff or rigid hydrogels takes long time and requires high level of enzymatic digestion, which may cause local toxicity or immune response [19].

The distribution of cell adhesive ligands is essential for integrin clustering and subsequent cell spreading. An interligand spacing < 70 nm in two dimensions is required for the formation of stable focal adhesions on stiff or rigid substrates [20, 21]. The unliganded integrins can be recruited and activated to bridge the nanopatterned adhesive points.[22] Controlling ligand spacing can regulate osteoblast maturation [23] and stem cell fate.[24] The order distribution of the nano-ligand also affects cell adhesion and differentiation [25, 26]. However, in these studies, cell osteogenic differentiation was still only achieved on stiff or rigid substrates. Recent work demonstrated that the increasing distance of cell adhesive ligands promotes the length of focal adhesions increased on soft substrates, while the adhesions collapse on stiff substrates. The individual integrin–ECM bonds (the molecular clutches) responsed to

force loading, recruited extra integrins, and thus generated more clutches on soft hydrogels with increasing ligand distance. This process redistributed the overall force among clutches to reduce the force loading per clutch [27]. Since the fate of stem cells is directly regulated by the focal adhesion induced mechanosensing [28], it would be interesting and reasonable to explore the cell mechanotransduction and differentiation behaviors on soft hydrogels with controllable ligand nanopatterns.

In this study, quasi-hexagonally arranged nanoarrays were employed to precisely control ligand distribution on physiologically stiff (about 30 kPa) and soft (about 3 kPa) hydrogels. The mechanoresponse and mechanotransduction of human mesenchymal stem cells (MSCs) were systematically studied for focal adhesion assembly, myosin motor activity, nuclear mechanics, ion channel activation, as well as the measurements of cellular traction forces. The spatial surface patterning of ligands at a distance of about 230 nm, which failed to support cell spreading on stiff hydrogels, was identified to promote cell adhesion and osteogenic differentiation on soft hydrogels to the comparable level as on stiff hydrogels. Our study is a breakthrough in bone tissue engineering, which opens a new route to design tailor-made biomaterials.

2. Experiment process

2.1. Preparation of Nanostructured Substrates.

Commercial glass coverslips (24 mm × 24 mm × 0.15 mm, Carl Roth & Co. GmbH Germany,) were cleaned with piranha solution (H_2SO_4:H_2O_2=3:1) for 4 h. After

washing with Milli-Q water for 3-5 times (Milli-Q Millipore System, USA), the coverslips were dried with N_2.

2.2. Preparation of Au Nanoparticle (AuNP)-Decorated Glass Coverslips.

AuNP array was determined by both speed and polymer block size, which has been sufficiently studied in our previous publications [29, 30]. Thus, we only used the determined parameters to fabricate the AuNPs with required spacing in this study and focused on the cell responses to the ligand spacing. Briefly, block copolymer PS(288)-b-P2VP(119) was stirred overnight in dry o-xylene under atmospheric condition. Then, the $HAuCl_4 \cdot 3H_2O$ precursor was added (loading amount, L=0.5, L = units($HAuCl_4$)/units(P2VP)), and the solution was kept stirring overnight to obtain the Au loading micellar solution. Clean coverslips were spin-coated with the micellar solution and etched by plasma with W10 (10% hydrogen and 90% argon) in a Tepla PS210 microwave plasma system (PVA Tepla, Germany). The lateral distance between AuNPs was adjusted to 30 nm by varying the velocity of the spin-coating process. The block copolymers, PS(1200)-b-P2VP(556) (L=0.4), PS(3120)-b-P2VP(875) (L=0.3), PS(5348)-b-P2VP(713) (L=0.5), were used for the nanoarray-decorated coverslips with lateral distances of 70 nm, 150 nm, 230 nm between AuNPs.

2.3. Transfer of Nanopatterns to polyacrylamide Gels.

The fabrication of AuNPs decorated polyacrylamide (PAM) hydrogels was performed according to a protocol similar to our previously method [26]. Glass slides decorated with quasi-hexagonal gold nanoarrays were immersed in 10 mM N, N'-bis(acryloyl)cystamine ethanol solution at the dark condition for 4 hour, and washed thoroughly with pure ethanol. The glass-bottom dishes (diameter 10 mm) were incubated in mixed solution of acetic acid, 3-(trimethoxysilyl)propyl methacrylate (Sigma) and ethanol (1/1/14), and washed three times with 96% ethanol. A solution containing 10% ammonium persulphate, 0.05% tetramethylethylenediamine (Sigma), and fluorescent 500-nm green carboxylated nanobeads (only for TFM test) was mixed with acrylamide and bis-acrylamide in different concentrations to make hydrogels with different stiffness. After drying both nanoarrays and acrylate-modified glass with N_2, 10 μL of this solution were then dipped in the center of AuNP patterned glass and covered with acrylate-modified glass. After 20 min of gel polymerization, the samples were soaked in phosphate-buffered saline (PBS) and incubated in the oven for 72 hours at 37°C, allowing them to swell. The substrate glass of the AuNPs were carefully removed from the glass to the hydrogels and the samples were gently immersed in PBS for sufficiently cleaning. The cyclo-RGDfK used in our study mimics the loop of the cell binding domain present in fibronectin [31], which has been proven to have high affinity to αvβ3 and α5β1 integrins [32-34]. Thus, hydrogels with nanopatterned AuNP were incubated with 25 μM cRGD-thiol (cyclic (RGDfK)-$(PEG_5)_2$-C, PCS-31062-PI, Peptides International) overnight at 4°C. Afterwards, cRGD-conjugated nanopatterned

hydrogels were washed five times with PBS (for at least 10 min each time) to remove unbound peptides before cell seeding.

2.4. Stiffness Measurements.

The stiffness of the hydrogels was measured using a rheometer (Kinexus, Malvern, USA) at 25 ℃. The parameters were setted as follows, the preload force was about 0.2 N, the shear strain was 1% and the frequency was 1 Hz.

2.5. Scanning Electron Microscopy (SEM).

Surfaces with AuNP patterns were sputtered with carbon (low-vacuum coater EM ACE200, Leica) and imaged by SEM (Leo1530, Zeiss) with an in-lens detector and 5 kV acceleration voltage. PAM hydrogels embedded AuNP arrays were vitrified and mounted in a liquid-nitrogen-cooled stage, before being transferred to a freeze-fracture system (EM BAF060, Leica). Samples were cooled to -90°C and kept in vacuum for 45 min to sublimate the water at the interfaces. Samples were then coated with carbon and transferred to the cryo-SEM (Ultra 55 FE-SEM, Zeiss) by an evacuated liquid-nitrogen-cooled shuttle (BAL-TECH VLC 100). Images were recorded at low-temperature conditions (T = −130 ± 5°C) and low acceleration voltages of 1–1.5 kV due to the low conductivity of the samples. The obtained electron micrographs were analyzed by ImageJ (National Institutes of Health) to measure the distance between a gold nanoparticle and its 6-nearest neighbours.

2.6. Cell Experiments.

Human Mesenchymal Stem Cells (hMSCs) were cultured in Dulbecco's modified Eagle's medium (Gibco, 21885-025) with 10% foetal bovine serum (FBS), 1% penicillin streptomycin, and maintained at 37°C in a humidified atmosphere with 5% CO_2. The osteogenic induced medium (A10069-01) and adipogenic induced medium (A10070-01) were obtained from Gibco. The cells were passaged once a week according to the standard protocols. The fifth to seventh passages of MSCs were used in this study.

Prior to cell seeding, the AuNP functionalized hydrogels were sterilized with UV light for 10 min and then washed twice with sterilized PBS and once with media. After being treated with 0.05% trypsin- EDTA (Gibco, Thermo Fisher Scientific, USA), centrifuged, and resuspended in culture media, cells were seeded to the surfaces of the hydrogels and maintained under standard culture condition.

2.7. Immunofluorescent Staining.

Samples were washed twice with PBS (pH=7.4), followed by fixing with 4% paraformaldehyde (Sigma, Germany) at room temperature for 15 min. Then, the samples were washed three times with cold PBS and treated with 0.25% (v/v) Triton-X 100 (Sigma, Germany) in PBS for 10 min at room temperature, followed by washing with PBS to remove the remains. The samples were then incubated with 1% (w/v) bovine serum albumin (BSA) in PBST (0.1% v/v Triton-X 100 in PBS) at room

temperature for 45 min to block nonspecific antibody binding. After briefly washing with PBST, the samples were incubated with the primary antibody in PBST with 1% BSA for 1 h at room temperature. The primary antibodies were used as follows: mouse monoclonal [clone 349] paxillin (610052, DB biosciences, 1:200 dilution), rabbit polyclonal anti-YAP (4912S, cell signaling technology, 1:200 dilution), rabbit monoclonal anti-Phospho-Myosin IIa (ser 1943, D7Z7T, cell signaling technology, 1:200), mouse monoclonal anti-Lamin A + C (mab636, NB100-74451, Novus Biologicals, 1:200). Afterward, the samples were washed twice with PBST and three times with PBS and were then incubated in the dark for another 1 h in a mixed solution of Alexa Fluor 488 phalloidin (1:1000 dilution, Life Technologies, Thermo Fisher Scientific, USA), anti-rabbit secondary antibody fluorescent dye Alexa Fluor 568 (1:200 dilution, A11011, Invitrogen, Germany), and anti-mouse secondary antibody fluorescent dye Alexa Fluor 647 (1:200 dilution, A21235, Life Technologies, Thermo Fisher Scientific, USA) in PBST with 1% BSA. Finally, the samples were washed twice with PBS and imaged under an inverted fluorescence microscope (Axiovert 200 M or an Imager. Z1, Germany). All acquired images were handled as 16-bit files and processed with the software Image J to adjust image settings and create the overlay fluorescence images.

2.8. Traction Force Microscopy (TFM).

AuNP functionalized PAM hydrogels containing 0.5 μm fluorescent carboxylated polystyrene beads (latex beads, carboxylate-modified polystyrene, fluorescent green, Sigma) were fabricated as previously described.[35] The beads were mixed in the hydrogel precursors and sunk during polymerization due to their own weight. After converting the hydrogels, the micro-beads were kept near the surface of the hydrogels. After immobilization of RGD peptide, the cells were seeded on the hydrogels. Fluorescent microscopy was used to take images of beads as well as spread cells.

Finally, the cells were removed by treating with 1% SDS for 10 min on the microscopy stage. The images were utilized for defining the original position of the dye-labeled beads.

ImageJ plugin "Align slices in stack" was used to correct the experimental drift of the samples. The displacement field in a spread cell region was subsequently calculated by a "particle image velocimetry" plugin in ImageJ. The obtained result was reconstructed using the "Fourier transform traction cytometry" plugin in order to generate the traction force field as a vector plot.

2.9. Ca^{2+} concentration

Fluo-4 AM (4 μM) was used for Ca^{2+} staining after the cells were cultured on the substrates for 24 h. The fluorescent intensity was marked as F. Moreover, Moreover, the fluorescent intensity of Fluo-4 AM that did not enter into the cell was marked as F_0. The related fluorescent intensity of Ca^{2+} in the cells was defined as $\Delta F/F_0$, where $\Delta F=F-F_0$ [36]. The detail procedure was followed the manufacturer's protocol. Cells were then

washed with Hanks' Balanced Salt Solution and then the fluorescent signals were captured by Inverted Zeiss Axiovert 200 M.

2.10. MSC Differentiation.

The MSCs were seeded on the hydrogels surfaces with density of 6000 cell/cm^2 in growth media for 1 day. Afterwards the cells was cultured in three different medium conditions, including osteogenic and adipogenic mixed (1:1) induction media for 7 days, growth media for 4 weeks, and adipogenic differentiation media for 2 weeks, respectively. The media were replaced every 3 days.

Alkaline phosphatase (ALP) was recognized as the biomarkers to examine cells osteogenic differentiation. The cells were stained by Leukocyte Alkaline Phosphatase Kit based on Naphthol AS-BI and fast blue BB salt (86C, Sigma-Aldrich). The detailed procedure was followed the manufacturer's protocol. The detailed procedure was followed the manufacturer's protocol. DAPI was then added to track the nuclei. The stained cells were observed in the inverted fluorescence microscope (Axiovert 200 M or an Imager. Z1, Germany) mounted with a color camera. The ratio of osteogenic differentiated cells on different hydrogels were calculated by counting the number of cells at least in five randomly selected fields (10X magnification) and normalizing to the total number of cells detected by DAPI staining.

Alizarin Red S was also used to analyze the late stage of cell osteogenic differentiation. The MSCs were seeded on the hydrogels surfaces with density of 6000

cell cm^{-2} in growth media for 1 day. Afterwards the media was replaced by osteogenic induced media for 15 days, and the media was replaced every 3 days. After removing the media, and the cells were gently washed with PBS for two times. The cells were then fixed with 4% paraformaldehyde for 15 minutes at room temperature, before washing with diH_2O three times to eliminate the Ca^{2+} in the hydrogels. Cells were further stained with 1 mL 0.5% alizarin red solution at room temperature for 30 minutes. The cells were washed with ddH_2O for 5 times and stained with DAPI. The results were obtained according to the methods described above in ALP section.

2.9.10. Statistical Analysis

All statistical analyses were performed with GraphPad Prism 8. Group differences were conducted by one-way ANOVA with Tukey's post -hoc test. P-values < 0.05 were considered as statistically significant (*p < 0.05, **p < 0.01, ***p < 0.001, ****p < 0.0001). Data are represented as mean ± standard deviation (S.D).

3. Results

3.1. Hydrogels with controllable stiffness and ligand spacing.

The hydrogels presenting hexagonally nanopatterned ligands were fabricated via a transfer strategy. The fabrication procedure was illustrated in **Figure 1a**. The hexagonally ordered gold nanoparticle arrays were fabricated via block copolymer micelle nanolithography (BCMN) on glass coverslips, which were further transferred to the polyacrylamide (PAM) hydrogels (detailed process in Materials and Methods).

The cyclic RGDfK was then immobilized onto the nanopatterns. The distance between the nanoparticles was adjusted by the chain length of block copolymers. The distance about 30, 70, 150, and 230 nm was designed (**Figure 1c,** Figure S1, and Table S1) to precisely control the distribution of RGD ligands. The size of a single gold nanoparticle is approximately 8 nm. Since integrin dimers have a lateral size of approximately 12 nm [20, 37, 38], one nanoparticle could only activate a single integrin dimer.

The stiffness of the hydrogels was controlled by varying the concentration of monomer and cross-linker. By adjusting the contents of monomer and cross-linker, the PAM hydrogels with different mechanical properties were prepared on the gold nanoparticle arrays to transfer the nanoparticles. The storage modulus G‘ was about 3 and 30 kPa (**Figure 1b**, Table S1, and Figure S2), mimicking the stiffness of adipose and osteoid tissue, respectively [16, 17]. The swelling of these hydrogels was not observed. The distance of the nanoparticles was not obviously increased after transfer (**Figure 1c** and **e**). In order to investigate the transfer process, the nanoparticles on glass coverslips were imaged before and after transfer. A boundary of nanoparticle array with highest tested density (distance at about 30 nm) was detected under SEM (**Figure 1d**). Almost no nanodots left in the area attached by soft hydrogels (left in image), suggesting the removal of nanoparticles by hydrogels. The hydrogel surfaces with transferred gold nanoparticle arrays were further imaged by cryo-SEM. As shown in **Figure 1e and S3**, the spacing of the nanodots on hydrogels was a little larger than that on glass surfaces due to hydrogel swelling. The deformation also slightly disordered

the nanopattern. The tendency of the nanodot distance on different samples was still maintained after transfer, the distance of nanodots on the hydorgels was summarized in **Table S1**.

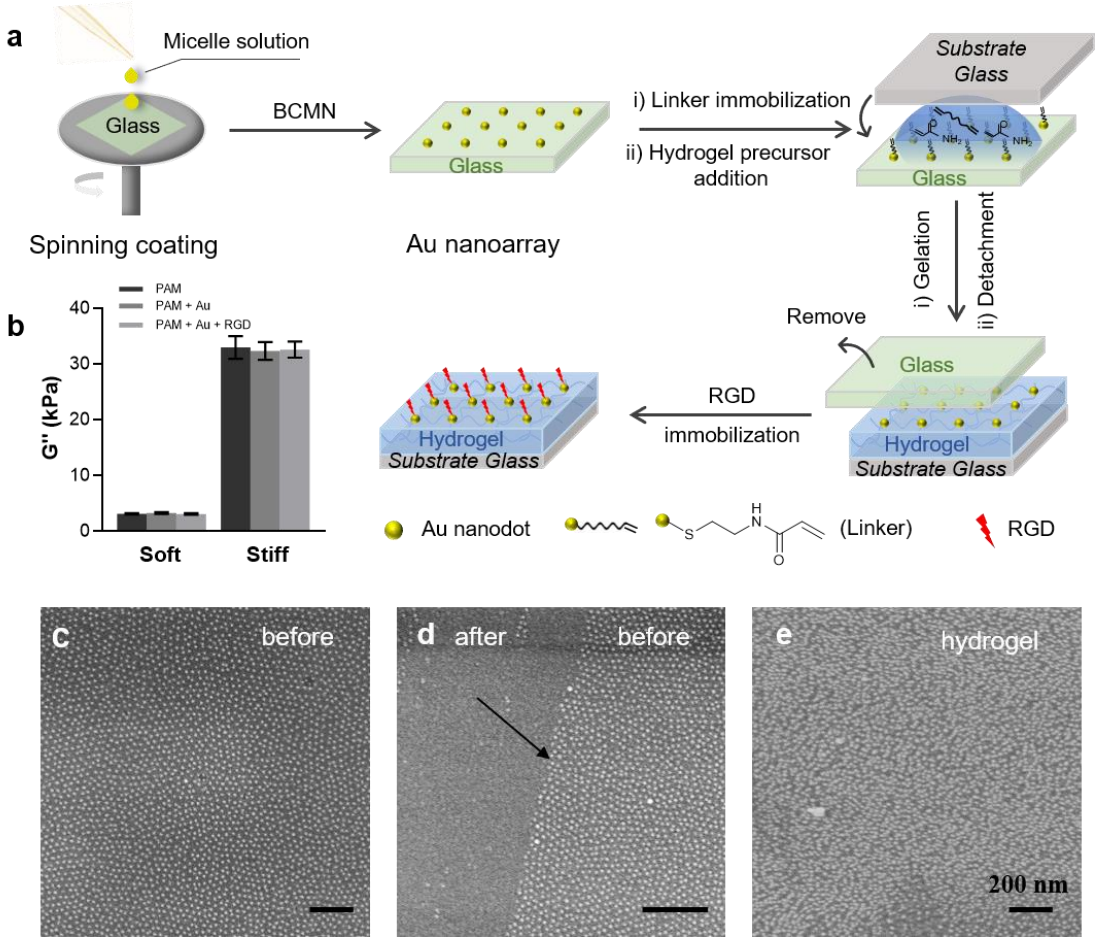

Figure 1. Hydrogels with controllable stiffness and ligand spacing. (a) Schematic illustration of the preparation of polyacrylamide (PAM) hydrogels with controllable ligand spacing. The hexagonally ordered gold nanoparticle array were fabricated via block copolymer micelle nanolithography (BCMN) on glass coverslips, and were further transferred to the polyacrylamide (PAM) hydrogels (detailed process in Materials and Methods). The cyclic RGDfK was then immobilized onto the

nanopatterns. The distance between the nanoparticles was adjusted by the chain length of block copolymers. (b) Average modulus of soft and stiff pristine PAM hydrogels or hydrogels functionalized with AuNPs and RGD peptides (3 technical replicates). SEM images of gold nanoparticle arrays with interparticle distance of 30 nm on glass coverslips (c) before and (d) after transfer to soft PAM hydrogels (about 3 kPa). Note that the hydrogel was only fabricated and removed on the left half of the glass coverslip in (d). (e) Cryo-SEM image of gold nanoparticle arrays with interparticle distance 30 nm on the soft hydrogels. Scale bar 200 nm.

3.2. Cell spreading and focal adhesion assembly are regulated by ligand spacing and substrate stiffness

Cell adhesion is directly related to the cytoskeleton formation [39-41]. The MSCs were stained with filamentous actin (F-actin) after 24 h on the RGD nanopatterned hydrogels. As shown in **Figure 2a** and **c**, the smaller ligand distance promoted cell spreading on the stiffness hydrogels, but larger distance promoted cell spreading on the soft hydrogels. The area reached about 6000 μm^2 on the surface with 30 nm ligand distance and decreased with the increasing ligand distance on 30 kPa hydrogels. Oppositely, the cell spread area increased stepwise with the increasing interligand distance on 3 kPa hydrogels, and was 600 and 4000 μm^2 for the distance 30 and 230 nm, respectively. In addition, aligned F-actin could be observed in well spread cells. Long actin filaments were not detectable on the soft hydrogels with the ligand distance of 30 and 70 nm.

Free cRGD (20 nM) was added in media during cell culture to inhibit integrin-based adhesion. As shown in **Figure S4**, cell adhesion failed regardless of ligand spacing and hydrogel stiffness in the presence of free cRGD. Therefore, cell adhesion and spreading on hydrogels were induced by specific integrin-ligand interaction.

Focal adhesions (FAs), which serve as the linkages between cells and microenvironment, transmit the environmental physical cues into cells and initiate mechanotranduction pathways [42, 43]. Therefore, the FA assembly on the hydrogels with different ligand space and stiffness was analyzed by immunostaining of paxillin. As shown in **Figure 2b** and **d**, the assembled FAs were mostly detected near cell periphery. The average FA length reached about 3.5 μm on the soft hydrogels with 230 nm ligand distance, and decreased significantly when the distance was reduced. The trend of FA formation was inverted on the stiff hydrogels.

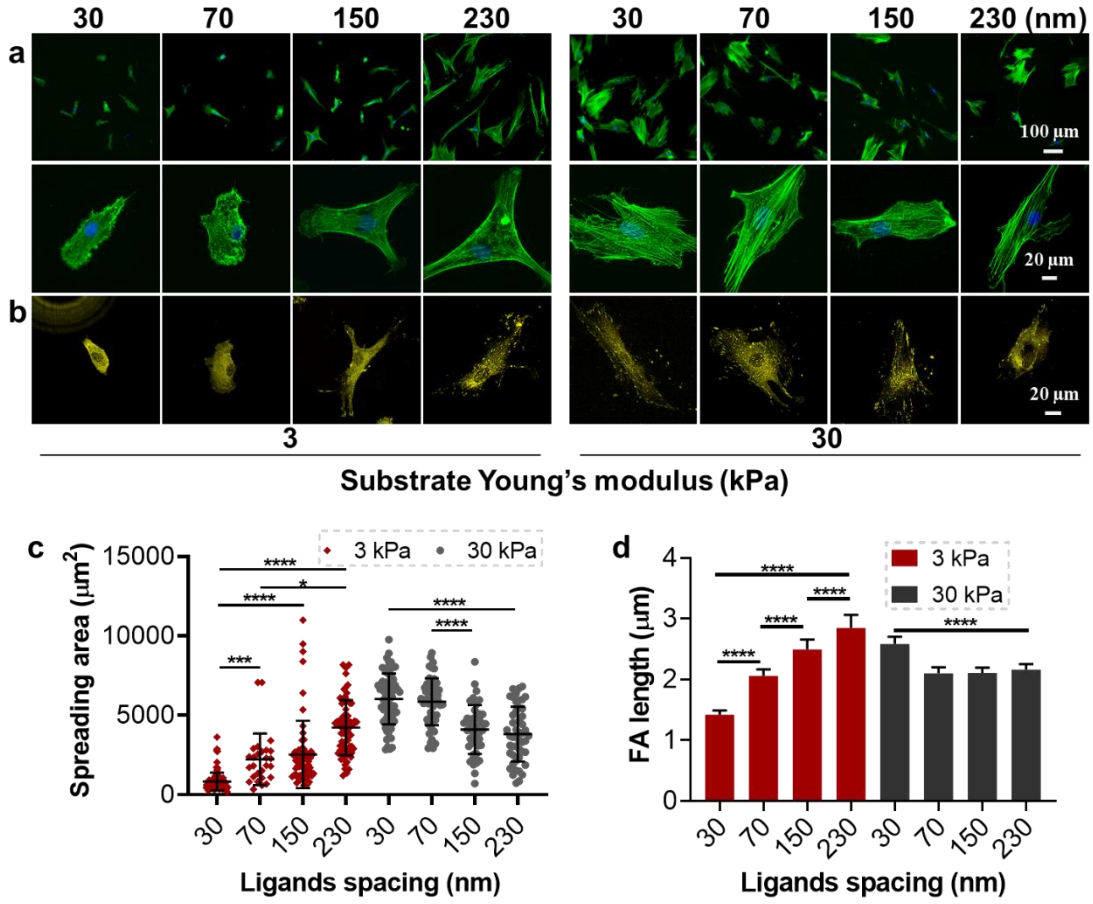

Figure 2. Cell adhesion on RGD-nanopatterned PAM hydrogels. (a) Fluorescence images of stained F-actin (green) and nucleus (blue) in cells cultured on the substrates for 24 hours. (b) Fluorescence images of cells stained for paxillin after 24 hours in culture. (c) Cell spread area after 24 hours (n = 60, 3 independent experiments). (d) Length of focal adhesion in cells after 24 hours (n = 15, 2 technical replicates).

3.3. Myosin II-dependent cell contractile forces mediate mechanosensing on nanopatterned hydrogels

Actomyosin contractility is the key regulator for cellular mechanotransduction, and directly related to cytoskeleton assembly and cell adhesion [44]. The role of myosin II

activity on cellular response to substrate stiffness and ligand spacing was therefore explored. The phosphorylation of myosin II was first analyzed by immunostaining with phospho-myosin IIa (Ser1943) antibodies (**Figure 3a** and **d**). The phosphorylation was promoted by the large ligand spacing on the soft hydrogels but small ligand spacing on the stiff hydrogels, which was consistent with the trend of cell adhesion. To further confirm the function of myosin II, the cells were treated with blebbistatin, a myosin II inhibitor. As shown in **Figure 3b** and **e**, the difference of cell adhesion induced by stiffness and ligand spacing was not observed after blebbistatin treatment. The assembly of actin cytoskeleton was absolutely limited and the cells spread area changed to the same level (3000 μm^2) in all conditions. Therefore, the myosin II-based cellular tension mediated cellular mechanosensing on ligand nanopatterned hydrogels.

Interestingly, the cell spread area increased after blebbistatin treatment on soft hydrogels with ligand space of 30 nm. Cells spread on the matrix with two mainly different ways, intracellular force dependent and independent ways. On the one hand, inhibition of myosin II attenuates the contractile force of actomyosin, which is critical for the mechanical signal transduction process caused by the ligands distance or substrate stiffness [27]. Thus, the cell spread area on the soft hydrogel with large distance ligands or stiff hydrogel decreased. On the other hand, inhibition of myosin II reduced actin retrograde flow. Thus, the leading-edge membrane tension increases to induce the formation of lamellipodia and filopodia, which widens the cell periphery

[45]. The intracellular force is already very limited in the cells on soft hydrogels with small ligand space, so the myosin II inhibition mainly exhibits the latter effects.

Since the myosin II-based cellular force acts upon ECM and substrate materials [35, 46], the force was further investigated by traction force microscopy employing fluorescently labeled beads embedded in PAM hydrogels. The cells adhering on the hydrogels could deform the substrates and cause a displacement of the embedded beads; this was recorded by microscopy to calculate cellular traction force. As shown in **Figure 3c** and **f**, large ligand spacing resulted in the enhanced traction force, while small ligand spacing limited force generation on the soft hydrogels. The mean traction force ranged from about 20 to 200 Pa on the soft hydrogels with ligand distance from 30 to 230 nm. On the stiff hydrogels, the traction force was in general larger than on the soft hydrogels. However, the highest force was generated on the surface with smallest ligand spacing (30 nm). The increased spacing limited the force generation. The frequency distribution of the traction force was also provided in **Figure S7**. The distribution of traction force gradually shifted to larger value on the soft hydrogels with increasing ligand distance, while the opposite trend was observed on the stiff hydrogels. The results of the traction force microscopy clearly show the force-dependent cell adhesion on the hydrogels with controllable ligand spacing.

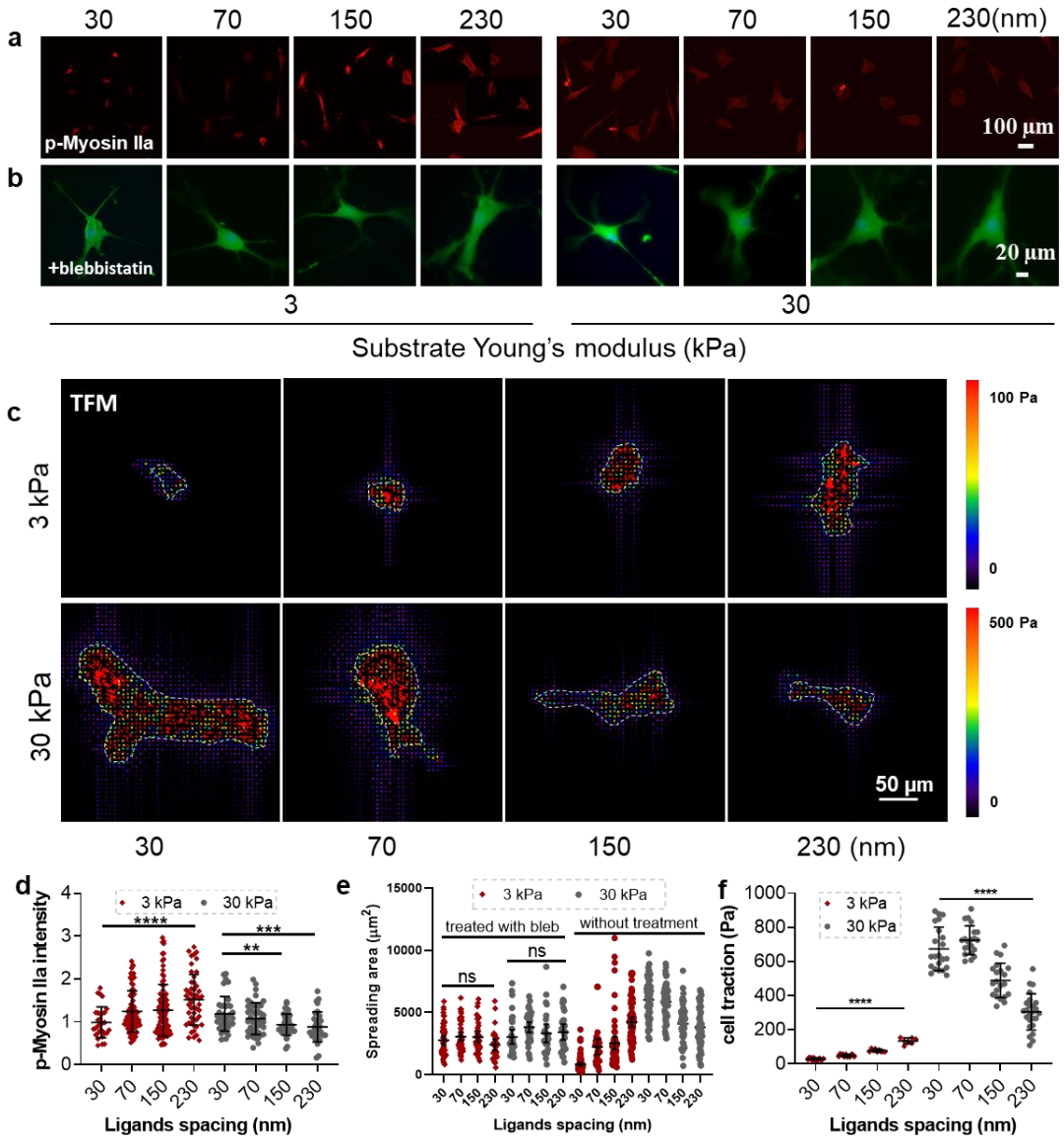

Figure 3. Myosin II-based cellular force generation. (a) Fluorescence images of cells immunostained for phospho-myosin IIa (Ser1943) after being cultured for 24 hours. The high resolution images were shown in Figure S5. (b) Fluorescent microscopy images of cells stained for F-actin (green) after being treated with 20 μM blebbistatin for 24 hours. More treated cells were shown in Figure S6. (c) The traction fields of a single cell adhered on ligand nanopatterned PAM hydrogels with embedded fluorescent beads after 24 hours. (d) The relative total fluorescent intensity of stained phospho-myosin IIa (Ser1943) in cells after 24 hours (n = 30, 2 technical replicates). (e) Cell

spread area after being treated with 20 μM blebbistatin for 24 hours (n = 25, 2 technical replicates). The cell area without blebbistatin treatment from Figure 2c was added for comparison. (f) Mean traction force of different single cells after being cultured for 24 hours (n = 15, 2 technical replicates).

3.4. Cell nuclear mechanics and nuclear chromatin organization are affected by ligand spacing and substrate stiffness

The cytoskeleton is linked to the nucleus through the linker of nucleus and cytoskeleton (LINC) complexes on the nuclear membrane [47]. Cytoskeletal tension can be transmitted from cytoplasm to the nucleus, causing nuclear deformation and altering the conformation of DNA or chromatin structures, as well as transcriptional activities [48]. The actin cap, which is composed of highly contractile actomyosin filament bundles that continuously bend to cover the top of the nucleus, is directly connected to the nuclear membrane for regulating nuclear shape [47]. The actin cap on both soft and stiff hydrogels was imaged and shown in **Figure 4a**. The fibers were disrupted and almost disappeared, when cells were cultured on soft hydrogels with ligand distances of 30 and 70 nm. The fibers emerged and the length increased with the increasing ligand distance. On stiff hydrogels, clear cap fibers were observed but gradually decreased, when the ligand distance increased from 30 to 230 nm. The actin cap generated tension can change the nuclear morphology [49]. The nuclear area was calculated in **Figure 4d**, which responding to the formation of actin cap. Strong actin cap fibers generated high

tension to compress the nucleus and increase the nuclear area. These results indicated the transmission of actomyosin-based cellular tension to the cell nucleus.

Cell nuclear mechanics was therefore investigated by immunostaining of nuclear skeleton lamin A/C. The expression and organization of lamin A/C reflect the nuclear stiffness and tension [50]. High tension inhibits the phosphorylation and further degradation of lamin A/C [51]. As shown in **Figure 4b**, deep wrinkles formed on the nuclear surface, when cellular tension was limited on the soft hydrogels with small ligand distance, i.e. 30 and 70 nm. The nuclear surfaces were getting smooth and the fluorescent intensity of the stained lamin A/C increased with the increasing ligand distance. On the stiff hydrogels, all of the nuclear surfaces were relatively smooth, but the fluorescent intensity decreased gradually with increasing ligand distance. These results demonstrate the response of cell nuclear mechanics to ligand nanopatterns on stiffness tunable hydrogels.

In addition, cell actin cap was disrupted with low concentration of latrunculin B (1 μM) to block cytoskeleton connection to nucleus [52]. Although the basal stress fibers were almost not affected (**Figure S8 a and b**), latrunculin B treatment decreased the amount of nuclear skeleton lamin A/C to the same level in all conditions (**Figure S8 c and d**). The results indicated that the nucleoskeleton assembly is caused by the actomyosin-based traction force.

The heatmap of DAPI intensity was subsequently created in **Figure 4c**. The nuclei on soft hydrogels with small ligand distance exhibited higher fluorescence intensity confirming the trend of high degree of chromatin condensation and low nuclear mechanics, which is consistent with previous studies [53, 54]. In line with lamin A/C-based nuclear tension, the nuclei exhibited overall low intensity when high level of

lamin A/C was detected. This indicates that chromatin was efficiently deformed in the stiff nucleus. Thus, cell mechanosensing induced by ligand spacing and substrate stiffness, was physically transmitted into cell nucleus and affected chromatin organization.

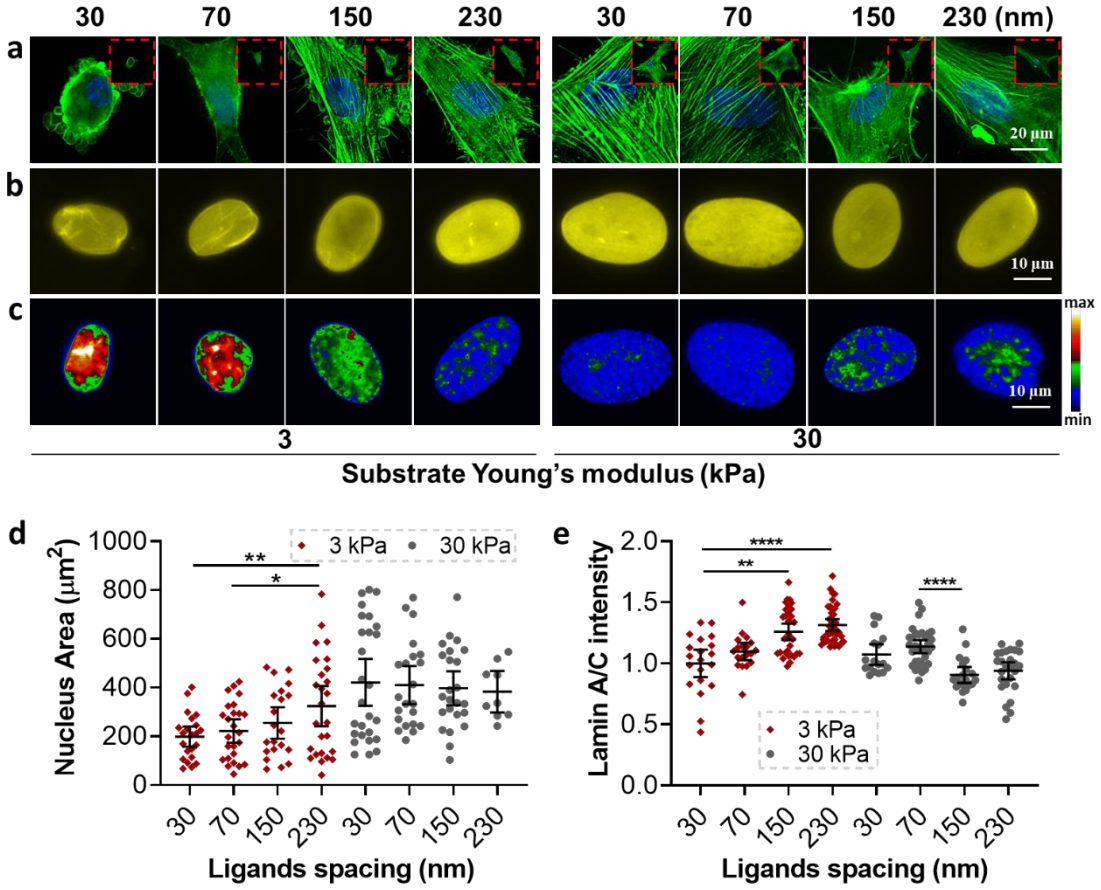

Figure 4. Cell nuclear mechanics regulated by ligand spacing and substrate stiffness. (a) Fluorescence images of the nuclear and perinuclear area of the cells stained for F-actin (green) and nucleus (blue) after being cultured for 24 hours. (b) Representative fluorescence images of cell nuclei stained for lamin A/C after 24 hours (n = 17, 2 technical replicates). (c) Representative heatmap of DAPI intensity of the cells after 24 hours. (d) Nuclear area of the cells after 24 hours (n = 15, 2 technical replicates). (e)

Relative average fluorescent intensity of lamin A/C of the cells (n = 18, 2 technical replicates).

3.5. Cell transcriptional activity and ion channel activation

The transcriptional regulators YAP/TAZ can regulate the expression of multiple mechanosensitive genes [55]. The subcellular distribution of YAP/TAZ responds to cytoskeleton tension and cell nuclear mechanics [50]. The generation of intracellular tension induces the shuttling of YAP/TAZ from the cytoplasm to the nucleus via the regulation of Ras-related GTPase RAP2 [56] and the ARID1A-containing SWI/SNF complex [57] as well as the tension-stretched nuclear pore opening [58]. Usually, only cells on stiff substrates exhibit nuclear localization of YAP/TAZ [59]. Here, the subcellular distribution of YAP/TAZ was investigated by YAP immunostaining (**Figure 5a, c**). As expected, YAP was mainly distributed in the cytoplasm when the ligand distance was 30 nm on soft hydrogels, but more concentrated in cell nucleus when the distance increased. In contrast, increasing ligand distance caused YAP deactivation from nucleus on stiff hydrogels. Therefore, cell transcriptional activity was synergistically regulated by ligand spacing and substrate stiffness.

Besides the transcriptional activity, the differentiation of MSCs is also mediated by the uptake of extracellular calcium ion [60]. Thus, the expression of ion channel transient receptor potential vanilloid-4 (TRPV4), which is widely expressed in osteoblasts [61], was investigated. As shown in **Figure 5b** and **d**, the activation of

TRPV4 matched cell spreading and tension generation. More TRPV4 was activated on soft hydrogels with ligand distance 230 nm. The results agreed with previous studies that TRPV4 could be activated in a force-dependent manner, triggered by either membrane stretching [62] or the force applied by β1 integrin [63].

The activation of TRPV4 was further investigated by quantifying the Ca^{2+} permeability (**Figure 5c and f**). The cells expressed more TRPV4 that indicated by immunostaining also obtained more Ca^{2+}. On the soft hydrogels, the Ca^{2+} intensity increased with the increasing ligand space. While on the stiff hydrogels, the intensity gradually decreased with the increasing ligand distance.

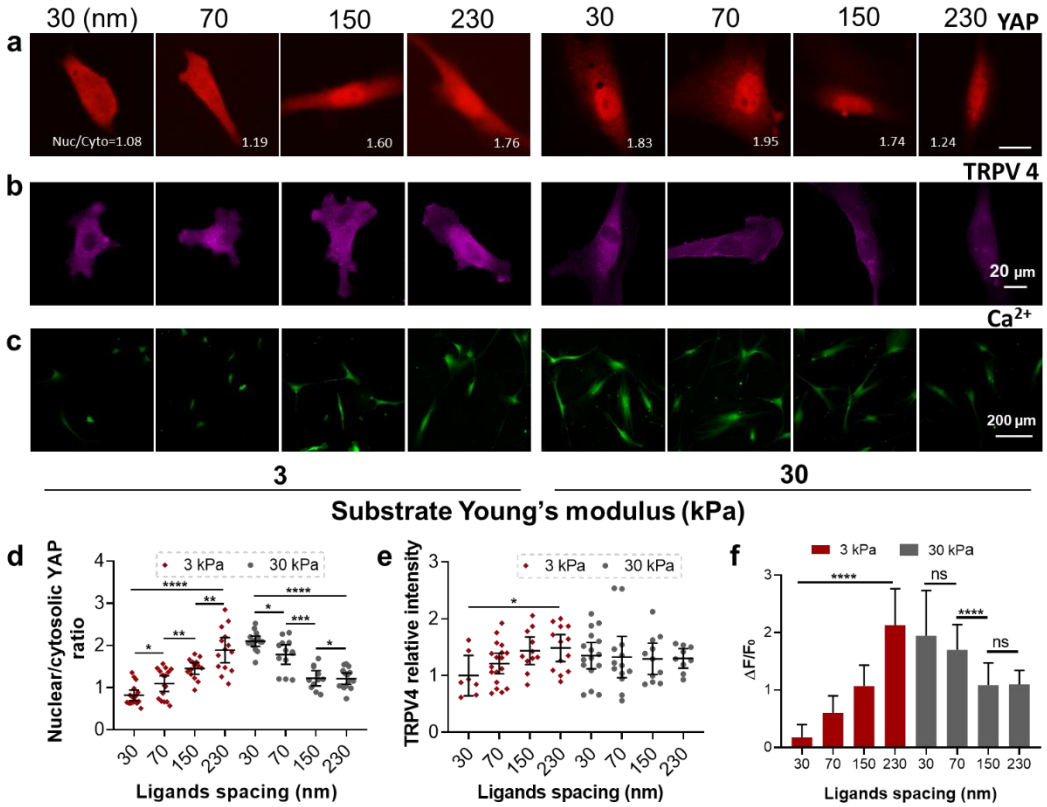

Figure 5. Cell transcriptional activity and ion channel activation. (a) Fluorescence images and (c) the related nuclear-to-cytoplasmic ratios of YAP for the cells after

cultured for 24 hours (n = 12, 2 technical replicates). The high resolution images were shown in Figure S9. (b) Fluorescence images and (d) related fluorescent intensity of the cells stained for TRPV4 after 24 hours (n = 10, 2 technical replicates). (c) Fluorescence images and (f) related fluorescent intensity for the cells stained for Ca^{2+} after cultured for 24 hours, where F is the fluorescence intensity of calcium ion in the cells and F_0 is the background fluorescence intensity of Fluo-4 AM. ($\Delta F=F-F_0$, n=50, 2 technical replicates).

3.6. Ligand spacing drives cell osteogenic differentiation on soft hydrogels

Osteogenic differentiation of stem cells can be regulated by mechanotransduction and ion channel activation. The up-regulated mechanotransduction and enhanced ion channel activation on soft hydrogels with large ligand space resulted in the high level of alkaline phosphatase (ALP) positive cells in multiple cell culture conditions, including in the 1:1 mix of osteogenic and adipogenic induction media for 1 week (**Figure 6a** and **b**), growth media for 4 weeks (Figure S10 a), and adipogenic induction media for 2 weeks (Figure S10 b). In mixed differentiation media, the ratio reached about 60% for ligand distance of 230 nm, while it was only 30% for the 30 nm distance. In comparison, the highest ratio of ALP positive cells was about 75% on the stiff hydrogels presenting inter-ligand distance of 30 nm, while the ratio decreased to 50% when the distance increased to 230 nm. The trend of the osteogenic differentiation of MSCs was similar in the growth media and the adipogenic induction media. The adipogenic differentiation of MSCs was investigated by oil red O staining was not

detectable in these conditions. This is because the bone marrow-derived MSCs used in our study have high tendency for osteogenic differentiation but low tendency for adipogenic differentiation.

The minerals deposition, late marker of osteogenic differentiation, was detected by imaging calcium deposition with Alizarin Red S (ARS). As shown in **Figure 6 c** and **d**, the ratio of ARS positive cells increased from 5% to 35% with the increasing ligand distance on the soft hydrogels, and the opposite tendency was observed on the stiffness hydrogels. These results together demonstrate that the osteogenic differentiation of MSCs on soft hydrogels could be promoted to the level comparable with that on stiff hydrogels by controlling ligand spacing.

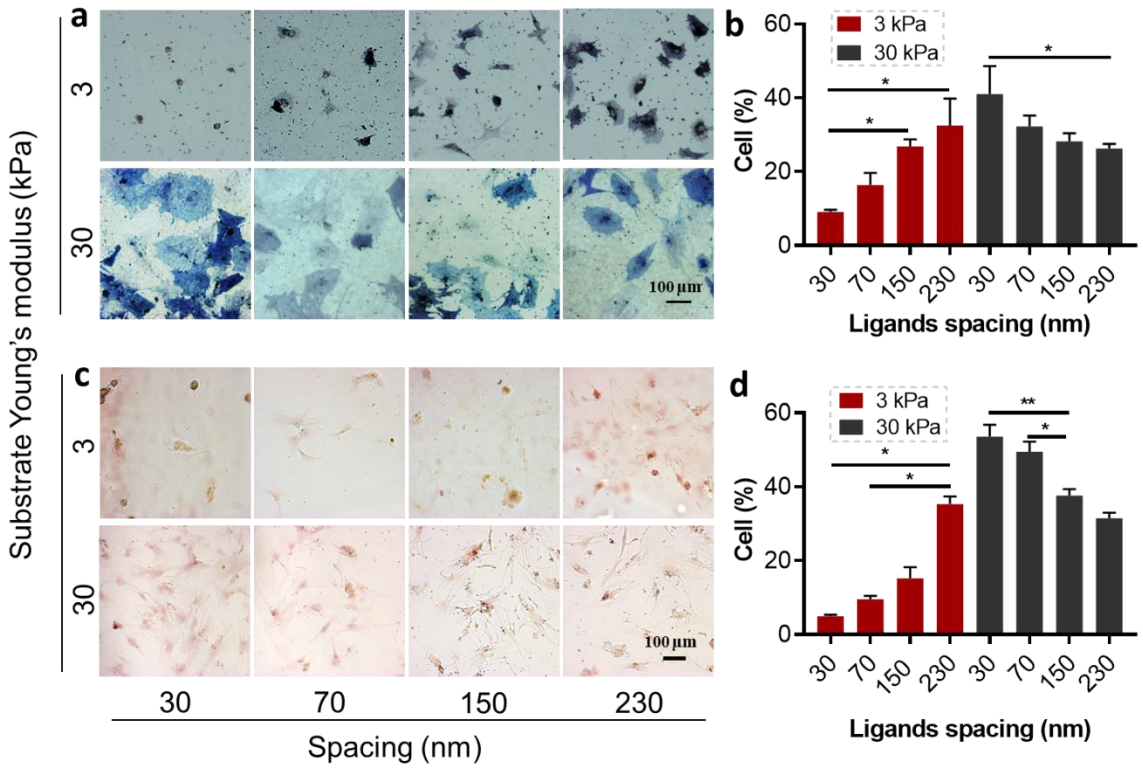

Figure 6. MSC osteogenic differentiation. (a) Representative micrographs of MSCs stained with ALP after cultured for 1 day in growth media and 6 days in the 1:1 mix of osteogenic and adipogenic differentiation media. (b) Quantitative ratio of ALP positive cells after 7 days in culture in differentiation media (n = 200, 2 technical replicates). (c) Representative micrographs of MSCs stained with ARS after cultured for 15 days in osteogenic differentiation media. (d) Quantitative ratio of ARS positive cells after cultured for 15 days in differentiation media (n = 35, 2 technical replicates).

4. Discussion

In the current view, only hydrogels with high stiffness and high ligand density are designed to promote cell adhesion and stem cell osteogenic differentiation [64, 65]. Strikingly, in the study presented here, soft hydrogels with large ligand spacing promote stem cell osteogenic differentiation. We systematically explored the entire force transmission pathway (**Scheme 1**). Force sensing at cell-materials interface was monitored thourgh focal adhesion formation and cytoskeleton assembly (**Figure 2**). The intracellular force generation in cell was analyzed through molecular motor myosin II and the traction force quantification (**Figure 3**). The force transmission into cell nucleus and genes were investigated through the formation of actin cap and nucleoskeleton as well as the gene distribution (**Figure 4**). The force-induced transcriptional activity was detected through YAP location (**Figure 5**). These results

together indicated the increased ligand spacing enhanced cell mechanosensing and mechanotransduction on soft hydrogels.

As shown in previous work, the increased ligand spacing results in the decreased number of individual integrin-ligand bonds, i.e. the molecular clutches [27]. Therefore, more myosin motors could distribute on one clutch to exert larger force per clutch[66]. When the force exerted on single clutches was above the threshold to unfold talin, an adaptor protein between actin filaments and integrin [67], the integrins could be recruited leading to adhesion growth. This recruitment promoted adhesion growth, which was supported by soft substrates. However, the growth rapidly reached maximum and the extra force loading caused adhesion collapse on stiff substrates [27]. Due to the enhanced force generation on single clutches of the MSCs adhered on the soft hydrogels with large ligand spacing, the nucleoskeleton lamin A/C was activated to increase the nuclear mechanics and trigger the activation of transcriptional regulators YAP/TAZ. Combined with the increased expression of ion channels, the osteogenic differentiation of MSCs was promoted on soft hydrogels to a level comparable to the one observed on stiff hydrogels. The osteogenic differentiation on such soft hydrogels was only achieved in very few reports. We recently achieved it on the soft hydrogels with large surface roughness [68, 69]. However, the high surface roughness increases the specific contact area between materials and biosystems, which might cause other unexpected immunoresponse *in vivo*.

This phenomenon was not detected in previously reported soft hydrogels with low density of randomly immobilized ligands [64, 65]. The ligand disordered distribution altered the stiffness regime for adhesion collapse [27]. Randomly immobilized ligands actually decreased the ligand distance in local, which limited the force generation on molecular clutches and the recruitment of extra integrins on soft hydrogels. Therefore, well-ordered ligand nanopatterns are required to promote cell adhesion and osteogenic differentiation on soft substrates.

Ding et al. also studied the synergistic effects of matrix stiffness and ligand spacings on stem cell fate determination [23, 70]. Interestingly, large ligand spacing (135 nm) on stiff (130 kPa) and rigid (3170 kPa) substrates limited cell adhesion but promoted stem cell osteogenic differentiation comparing with small ligand spacing (49 nm). It should be noted that the tested stiffness in these experiments was above the physiological stiffness that cells are sensitive to (< 100 kPa) [71]. We also examined cell adhesion and differentiation on hydrogels with such high stiffness and different ligand spacing. Our results are in agreement with Ding et al.'s results (data not shown). Unlike the presented hydrogels with physiological stiffness, YAP/TAZ were highly concentrated in cell nucleus even when cell adhesion was relatively limited on the rigid hydrogels with large ligand spacing (Data not shown). Our hypothesis is that the nuclear concentration of YAP/TAZ is above the required threshold on these rigid substrates with large ligand spacing, thus other factors appear to be determinant in mediating cell fate determination in this case. Nevertheless, this is out of the scope of the current study.

Actomyosin-based mechanotransduction and YAP/TAZ are still the dominant regulators as shown above for the cell differentiation on hydrogels with physiological stiffness in the present study.

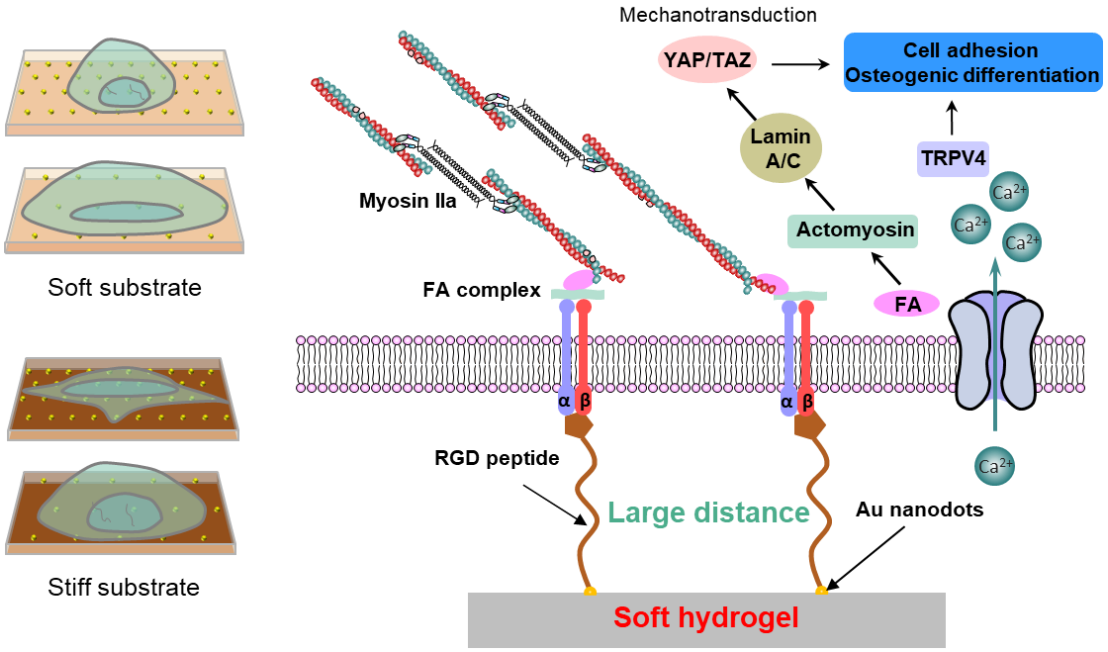

Scheme 1. Schematic illustration of the effects of ligands density on the surface of matrix and the force transmission process from the substrate to cell nucleus.

5. Conclusion

In this study, we developed the functional soft hydrogels with quasi-hexagonally arranged ligand nanoarray to stimulate cellular mechanotransduction and promote stem cell osteogeinc differentiation. The controllable ligand spacing initiates mechanotransduction pathways: focal adhesion formation – actomyosin assembly – nucleoskeleton assembly – activation of transcriptional regulators, as well as expression of ion channels. These factors synergize to drive the osteogenic differentiation of stem

cells on the 3 kPa soft hydrogels, which are usually expected to inhibit cell osteogenic differentiation. This unusual phenomenon can be explained by the optimized force loading on single molecular clutches to activate focal adhesion formation. Our study will provide new methods to regulate stem cell fate determination and extend the choice of biomaterials in regenerative applications.

Acknowledgments

We acknowledge the financial support from National Key R&D Program of China (Grant Nos. 2018YFC1106800, 2016YFC1103000 and 2018YFC1106400) and National Natural Science Foundation of China (Grant Nos. 51973129, 51773127 and 51873115), China Scholarship Council (the State Scholarship Fund) and Max Planck Society. E.A. Cavalcanti-Adam alo acknowledges the support from the European Union's Horizon 2020 research and innovation programme under the Marie Skłodowska-Curie grant agreement No 872869.

References

[1] F.-M. Chen, X. Liu, Advancing biomaterials of human origin for tissue engineering, Prog. Polym. Sci. 53 (2016) 86-168.
[2] C.M. Madl, S.C. Heilshorn, H.M.J.N. Blau, Bioengineering strategies to accelerate stem cell therapeutics, Nature 557(7705) (2018) 335-342.
[3] D.E. Discher, D.J. Mooney, P.W. Zandstra, Growth factors, matrices, and forces combine and control stem cells, Science 324(5935) (2009) 1673-1677.
[4] H. Kang, H.J. Jung, D.S.H. Wong, S.K. Kim, S. Lin, K.F. Chan, L. Zhang, G. Li, V.P. Dravid, L. Bian, Remote control of heterodimeric magnetic nanoswitch regulates the adhesion and differentiation of stem cells, J. Am. Chem. Soc. 140(18) (2018) 5909-5913.
[5] H. Chang, X.-Q. Liu, M. Hu, H. Zhang, B.-C. Li, K.-F. Ren, T. Boudou, C. Albiges-Rizo, C. Picart, J. Ji, Substrate Stiffness Combined with Hepatocyte Growth Factor Modulates Endothelial Cell Behavior, Biomacromolecules 17(9) (2016) 2767-2776.
[6] A.W. Holle, J.L. Young, K.J. Van Vliet, R.D. Kamm, D. Discher, P. Janmey, J.P. Spatz, T. Saif, Cell–extracellular matrix mechanobiology: forceful tools and emerging needs for basic and translational research, Nano Lett. 18(1) (2017) 1-8.
[7] H. Chang, M. Hu, H. Zhang, K.-f. Ren, B.-c. Li, H. Li, L.-m. Wang, W.-x. Lei, J. Ji, Improved Endothelial Function of Endothelial Cell Monolayer on the Soft Polyelectrolyte Multilayer Film with Matrix-Bound Vascular Endothelial Growth Factor, ACS Appl. Mater. Interfaces 8(23) (2016) 14357-14366.
[8] K.H. Vining, D.J. Mooney, Mechanical forces direct stem cell behaviour in development and regeneration, Nat. Rev. Mol. Cell Biol. 18(12) (2017) 728–742.
[9] M. Wang, B. Cheng, Y.W. Yang, H. Liu, G.Y. Huang, L.C. Han, F. Li, F. Xu, Microchannel Stiffness and Confinement Jointly Induce the Mesenchymal-Amoeboid Transition of Cancer Cell Migration, Nano Lett. 19(9) (2019) 5949-5958.
[10] Y. Hou, L. Yu, W. Xie, L.C. Camacho, M. Zhang, Z. Chu, Q. Wei, R. Haag, Surface Roughness and Substrate Stiffness Synergize To Drive Cellular Mechanoresponse, Nano Lett. 20(1) (2020) 748-757.
[11] D.E. Discher, P. Janmey, Y.-l. Wang, Tissue cells feel and respond to the stiffness of their substrate, Science 310(5751) (2005) 1139-1143.
[12] F. Chowdhury, S. Na, D. Li, Y.-C. Poh, T.S. Tanaka, F. Wang, N. Wang, Material properties of the cell dictate stress-induced spreading and differentiation in embryonic stem cells, Nat. Mater. 9(1) (2010) 82–88.
[13] T.H. Kim, D.B. An, S.H. Oh, M.K. Kang, H.H. Song, J.H. Lee, Creating stiffness gradient polyvinyl alcohol hydrogel using a simple gradual freezing–thawing method to investigate stem cell differentiation behaviors, Biomaterials 40 (2015) 51-60.
[14] A.J. Engler, S. Sen, H.L. Sweeney, D.E. Discher, Matrix elasticity directs stem cell lineage specification, Cell 126(4) (2006) 677-689.
[15] M. Guvendiren, J.A. Burdick, Stiffening hydrogels to probe short-and long-term

cellular responses to dynamic mechanics, Nat. Commun. 3 (2012) 792.
[16] D.E. Discher, P. Janmey, Y.L. Wang, Tissue cells feel and respond to the stiffness of their substrate, Science 310(5751) (2005) 1139-1143.
[17] D.A. Young, Y.S. Choi, A.J. Engler, K.L. Christman, Stimulation of adipogenesis of adult adipose-derived stem cells using substrates that mimic the stiffness of adipose tissue, Biomaterials 34(34) (2013) 8581-8588.
[18] J. Eyckmans, T. Boudou, X. Yu, C.S.J.D.c. Chen, A hitchhiker's guide to mechanobiology, Dev. Cell 21(1) (2011) 35-47.
[19] D. Kong, W. Megone, K.D. Nguyen, S. Di Cio, M. Ramstedt, J.E. Gautrot, Protein Nanosheet Mechanics Controls Cell Adhesion and Expansion on Low-Viscosity Liquids, Nano Lett. 18(3) (2018) 1946-1951.
[20] M. Arnold, E.A. Cavalcanti‐Adam, R. Glass, J. Blümmel, W. Eck, M. Kantlehner, H. Kessler, J.P. Spatz, Activation of integrin function by nanopatterned adhesive interfaces, Chemphyschem 5(3) (2004) 383-388.
[21] J. Deng, C.S. Zhao, J.P. Spatz, Q. Wei, Nanopatterned Adhesive, Stretchable Hydrogel to Control Ligand Spacing and Regulate Cell Spreading and Migration, ACS Nano 11(8) (2017) 8282-8291.
[22] R. Changede, H. Cai, S.J. Wind, M.P. Sheetz, Integrin nanoclusters can bridge thin matrix fibres to form cell–matrix adhesions, Nat. Mater. 18 (2019) 1366–1375.
[23] E.A. Cavalcanti-Adam, P. Tomakidi, M. Bezler, J.P. Spatz, Geometric organization of the extracellular matrix in the control of integrin-mediated adhesion and cell function in osteoblasts, Prog. Orthod. 6(2) (2005) 232-237.
[24] P. Han, J.E. Frith, G.A. Gomez, A.S. Yap, G.M. O'Neill, J.J. Cooper-White, Five piconewtons: the difference between osteogenic and adipogenic fate choice in human mesenchymal stem cells, ACS nano 13(10) (2019) 11129-11143.
[25] J. Huang, S.V. Grater, F. Corbellini, S. Rinck, E. Bock, R. Kemkemer, H. Kessler, J. Ding, J.P. Spatz, Impact of order and disorder in RGD nanopatterns on cell adhesion, Nano Lett. 9(3) (2009) 1111-1116.
[26] S.H.D. Wong, B. Yin, B. Yang, S. Lin, R. Li, Q. Feng, H. Yang, L. Zhang, Z. Yang, G. Li, Anisotropic Nanoscale Presentation of Cell Adhesion Ligand Enhances the Recruitment of Diverse Integrins in Adhesion Structures and Mechanosensing‐Dependent Differentiation of Stem Cells, Adv. Funct. Mater. 29(8) (2019) 1806822.
[27] R. Oria, T. Wiegand, J. Escribano, A. Elosegui-Artola, J.J. Uriarte, C. Moreno-Pulido, I. Platzman, P. Delcanale, L. Albertazzi, D. Navajas, X. Trepat, J.M. Garcia-Aznar, E.A. Cavalcanti-Adam, P. Roca-Cusachs, Force loading explains spatial sensing of ligands by cells, Nature 552(7684) (2017) 219–224.
[28] H. Wolfenson, B. Yang, M.P. Sheetz, Steps in mechanotransduction pathways that control cell morphology, Annu. Rev. Physiol. 81 (2019) 585-605.
[29] J.P. Spatz, V.Z.H. Chan, S. Mossmer, F.M. Kamm, A. Plettl, P. Ziemann, M. Moller, A combined top-down/bottom-up approach to the microscopic localization of metallic nanodots, Adv. Mater. 14(24) (2002) 1827-1832.
[30] V.C. Hirschfeld-Warneken, M. Arnold, A. Cavalcanti-Adam, M. Lopez-Garcia, H.

Kessler, J.P. Spatz, Cell adhesion and polarisation on molecularly defined spacing gradient surfaces of cyclic RGDfK peptide patches, Eur. J. Cell Biol. 87(8-9) (2008) 743-750.
[31] C. Mas-Moruno, R. Fraioli, F. Rechenmacher, S. Neubauer, T.G. Kapp, H. Kessler, alpha v beta 3-or alpha 5 beta 1-Integrin-Selective Peptidomimetics for Surface Coating, Angew. Chem. Int. Ed. 55(25) (2016) 7048-7067.
[32] A. Bochen, U.K. Marelli, E. Otto, D. Pallarola, C. Mas-Moruno, F.S. Di Leva, H. Boehm, J.P. Spatz, E. Novellino, H. Kessler, L. Marinelli, Biselectivity of isoDGR Peptides for Fibronectin Binding Integrin Subtypes alpha 5 beta 1 and alpha v beta 6: Conformational Control through Flanking Amino Acids, J. Med. Chem. 56(4) (2013) 1509-1519.
[33] T.G. Kapp, F. Rechenmacher, S. Neubauer, O.V. Maltsev, E.A. Cavalcanti-Adam, R. Zarka, U. Reuning, J. Notni, H.J. Wester, C. Mas-Moruno, J. Spatz, B. Geiger, H. Kessler, A Comprehensive Evaluation of the Activity and Selectivity Profile of Ligands for RGD-binding Integrins, Sci. Rep. 7 (2017) 39805.
[34] L.X. Yu, Y. Hou, W.Y. Xie, J.L.C. Camacho, C. Cheng, A. Holle, J. Young, B. Trappmann, W.F. Zhao, M.F. Melzig, E.A. Cavalcanti-Adam, C.S. Zhao, J.P. Spatz, Q. Wei, R. Haag, Ligand Diffusion Enables Force-Independent Cell Adhesion via Activating alpha 5 beta 1 Integrin and Initiating Rac and RhoA Signaling, Adv. Mater. 32(29) (2020) 2002566.
[35] J. Li, J. Di Russo, X. Hua, Z. Chu, J.P. Spatz, Q. Wei, Surface Immobilized E‐Cadherin Mimetic Peptide Regulates the Adhesion and Clustering of Epithelial Cells, Adv. Healthc. Mater. 8(8) (2019) 1801384.
[36] W. Echevarría, M.F. Leite, M.T. Guerra, W.R. Zipfel, M.H. Nathanson, Regulation of calcium signals in the nucleus by a nucleoplasmic reticulum, Nat. Cell Biol. 5(5) (2003) 440-446.
[37] J.-P. Xiong, T. Stehle, R. Zhang, A. Joachimiak, M. Frech, S.L. Goodman, M.A. Arnaout, Crystal structure of the extracellular segment of integrin αVβ3 in complex with an Arg-Gly-Asp ligand, Science 296(5565) (2002) 151-155.
[38] J.-P. Xiong, T. Stehle, B. Diefenbach, R. Zhang, R. Dunker, D.L. Scott, A. Joachimiak, S.L. Goodman, M.A. Arnaout, Crystal structure of the extracellular segment of integrin αVβ3, Science 294(5541) (2001) 339-345.
[39] D.R. Critchley, Focal adhesions–the cytoskeletal connection, Curr. Opin. Cell Biol. 12(1) (2000) 133-139.
[40] S.J. Soenen, N. Nuytten, S.F. De Meyer, S.C. De Smedt, M. De Cuyper, High intracellular iron oxide nanoparticle concentrations affect cellular cytoskeleton and focal adhesion kinase-mediated signaling, Small 6(7) (2010) 832-842.
[41] C.E. Turner, Paxillin and focal adhesion signalling, Nat. Cell Biol. 2(12) (2000) E231–E236.
[42] C.S. Chen, J.L. Alonso, E. Ostuni, G.M. Whitesides, D.E. Ingber, Cell shape provides global control of focal adhesion assembly, Biochem. Biophys. Res. Commun. 307(2) (2003) 355-361.

[43] B. Geiger, J.P. Spatz, A.D. Bershadsky, Environmental sensing through focal adhesions, Nat. Rev. Mol. Cell Biol. 10(1) (2009) 21-33.
[44] M. Murrell, P.W. Oakes, M. Lenz, M.L.J.N.r.M.c.b. Gardel, Forcing cells into shape: the mechanics of actomyosin contractility, Nat. Rev. Mol. Cell Biol. 16(8) (2015) 486-498.
[45] N.A. Medeiros, D.T. Burnette, P. Forscher, Myosin II functions in actin-bundle turnover in neuronal growth cones, Nat. Cell Biol. 8(3) (2006) 215-226.
[46] F.M. Watt, W.T. Huck, Role of the extracellular matrix in regulating stem cell fate, Nat. Rev. Mol. Cell Biol. 14(8) (2013) 467-473.
[47] O. Gay, B. Gilquin, F. Nakamura, Z.A. Jenkins, R. McCartney, D. Krakow, A. Deshiere, N. Assard, J.H. Hartwig, S.P. Robertson, J. Baudier, RefilinB (FAM101B) targets FilaminA to organize perinuclear actin networks and regulates nuclear shape, Proc. Natl. Acad. Sci. U. S. A. 108(28) (2011) 11464-11469.
[48] K.J. De France, F. Xu, T. Hoare, Structured macroporous hydrogels: Progress, challenges, and opportunities, Adv. Healthc. Mater. 7(1) (2018) 1700927.
[49] J.-K. Kim, A. Louhghalam, G. Lee, B.W. Schafer, D. Wirtz, D.-H. Kim, Nuclear lamin A/C harnesses the perinuclear apical actin cables to protect nuclear morphology, Nat. Commun. 8(1) (2017) 2123.
[50] J. Swift, I.L. Ivanovska, A. Buxboim, T. Harada, P. Dingal, J. Pinter, J.D. Pajerowski, K.R. Spinler, J.W. Shin, M. Tewari, F. Rehfeldt, D.W. Speicher, D.E. Discher, Nuclear Lamin-A Scales with Tissue Stiffness and Enhances Matrix-Directed Differentiation, Science 341(6149) (2013) 1240104.
[51] S. Cho, M. Vashisth, A. Abbas, S. Majkut, K. Vogel, Y. Xia, I.L. Ivanovska, J. Irianto, M. Tewari, K. Zhu, Mechanosensing by the lamina protects against nuclear rupture, DNA damage, and cell-cycle arrest, Dev. Cell 49(6) (2019) 920-935. .
[52] S.B. Khatau, C.M. Hale, P.J. Stewart-Hutchinson, M.S. Patel, C.L. Stewart, P.C. Searson, D. Hodzic, D. Wirtz, A perinuclear actin cap regulates nuclear shape, Proc. Natl. Acad. Sci. U. S. A. 106(45) (2009) 19017-19022.
[53] M.J. Salierno, L. Garcia-Fernandez, N. Carabelos, K. Kiefer, A.J. Garcia, A. del Campo, Phototriggered fibril-like environments arbitrate cell escapes and migration from endothelial monolayers, Biomaterials 82 (2016) 113-123.
[54] A.R. Killaars, J.C. Grim, C.J. Walker, E.A. Hushka, T.E. Brown, K.S. Anseth, Extended Exposure to Stiff Microenvironments Leads to Persistent Chromatin Remodeling in Human Mesenchymal Stem Cells, Adv. Sci. 6(3) (2019) 1801483.
[55] S. Dupont, L. Morsut, M. Aragona, E. Enzo, S. Giulitti, M. Cordenonsi, F. Zanconato, J. Le Digabel, M. Forcato, S. Bicciato, N. Elvassore, S. Piccolo, Role of YAP/TAZ in mechanotransduction, Nature 474(7350) (2011) 179–183.
[56] Z.P. Meng, Y.J. Qiu, K.C. Lin, A. Kumar, J.K. Placone, C. Fang, K.C. Wang, S.C. Lu, M. Pan, A.W. Hong, T. Moroishi, M. Luo, S.W. Plouffe, Y.R. Diao, Z. Ye, H.W. Park, X.Q. Wang, F.X. Yu, S. Chien, C.Y. Wang, B. Ren, A.J. Engler, K.L. Guan, RAP2 mediates mechanoresponses of the Hippo pathway, Nature 560(7720) (2018) 655–660.
[57] L. Chang, L. Azzolin, D. Di Biagio, F. Zanconato, G. Battilana, R.L. Xiccato, M.

Aragona, S. Giulitti, T. Panciera, A. Gandin, G. Sigismondo, J. Krijgsveld, M. Fassan, G. Brusatin, M. Cordenonsi, S. Piccolo, The SWI/SNF complex is a mechanoregulated inhibitor of YAP and TAZ, Nature 563(7730) (2018) 265-269.
[58] A. Elosegui-Artola, I. Andreu, A.E.M. Beedle, A. Lezamiz, M. Uroz, A.J. Kosmalska, R. Oria, J.Z. Kechagia, P. Rico-Lastres, A.L. Le Roux, C.M. Shanahan, X. Trepat, D. Navajas, S. Garcia-Manyes, P. Roca-Cusachs, Force Triggers YAP Nuclear Entry by Regulating Transport across Nuclear Pores, Cell 171(6) (2017) 1397-1410.
[59] G. Brusatin, T. Panciera, A. Gandin, A. Citron, S. Piccolo, Biomaterials and engineered microenvironments to control YAP/TAZ-dependent cell behaviour, Nat. Mater. 17(12) (2018) 1063-1075.
[60] A.M.C. Barradas, H.A.M. Fernandes, N. Groen, Y.C. Chai, J. Schrooten, J. van de Peppel, J. van Leeuwen, C.A. van Blitterswijk, J. de Boer, A calcium-induced signaling cascade leading to osteogenic differentiation of human bone marrow-derived mesenchymal stromal cells, Biomaterials 33(11) (2012) 3205-3215.
[61] H.-p. Lee, R. Stowers, O. Chaudhuri, Volume expansion and TRPV4 activation regulate stem cell fate in three-dimensional microenvironments, Nat. Commun. 10(1) (2019) 529.
[62] X. Gao, L. Wu, R.G. O'Neil, Temperature-modulated diversity of TRPV4 channel gating - Activation by physical stresses and phorbol ester derivatives through protein kinase C-dependent and -independent pathways, J. Biol. Chem. 278(29) (2003) 27129-27137.
[63] B.D. Matthews, C.K. Thodeti, J.D. Tytell, A. Mammoto, D.R. Overby, D.E. Ingber, Ultra-rapid activation of TRPV4 ion channels by mechanical forces applied to cell surface β1 integrins, Integr. Biol. 2(9) (2010) 435-442.
[64] A. Engler, L. Bacakova, C. Newman, A. Hategan, M. Griffin, D. Discher, Substrate compliance versus ligand density in cell on gel responses, Biophys. J. 86(1) (2004) 617-628.
[65] A.E. Stanton, X.M. Tong, S. Lee, F. Yang, Biochemical Ligand Density Regulates Yes-Associated Protein Translocation in Stem Cells through Cytoskeletal Tension and Integrins, ACS Appl. Mater. Interfaces 11(9) (2019) 8849-8857.
[66] A. Elosegui-Artola, R. Oria, Y. Chen, A. Kosmalska, C. Pérez-González, N. Castro, C. Zhu, X. Trepat, P.J.N.c.b. Roca-Cusachs, Mechanical regulation of a molecular clutch defines force transmission and transduction in response to matrix rigidity, Nat. Cell Biol. 18(5) (2016) 540.
[67] A. Kumar, M. Ouyang, K. Van den Dries, E.J. McGhee, K. Tanaka, M.D. Anderson, A. Groisman, B.T. Goult, K.I. Anderson, M.A. Schwartz, Talin tension sensor reveals novel features of focal adhesion force transmission and mechanosensitivity, J. Cell Biol. 213(3) (2016) 371-383.
[68] Y. Hou, L.X. Yu, W.Y. Xie, L.C. Camacho, M. Zhang, Z.Q. Chu, Q. Wei, R. Haag, Surface Roughness and Substrate Stiffness Synergize To Drive Cellular Mechanoresponse, Nano Lett. 20(1) (2020) 748-757.
[69] Y. Hou, W.Y. Xie, L.X. Yu, L.C. Camacho, C.X. Nie, M. Zhang, R. Haag, Q. Wei,

Surface Roughness Gradients Reveal Topography-Specific Mechanosensitive Responses in Human Mesenchymal Stem Cells, Small 16(10) (2020) 1905422.
[70] K. Ye, X. Wang, L. Cao, S. Li, Z. Li, L. Yu, J. Ding, Matrix stiffness and nanoscale spatial organization of cell-adhesive ligands direct stem cell fate, Nano Lett. 15(7) (2015) 4720-4729.
[71] J.H. Wen, L.G. Vincent, A. Fuhrmann, Y.S. Choi, K.C. Hribar, H. Taylor-Weiner, S. Chen, A.J. Engler, Interplay of matrix stiffness and protein tethering in stem cell differentiation, Nat. Mater. 13(10) (2014) 979-987.